OPEN ACCESS

University of BRISTOL

Rankin, AJ., Krauskopf, B., Lowenberg, MH., & Coetzee, EB. (2010). *Nonlinear analysis of lateral loading during taxiway turns*. http://hdl.handle.net/1983/1596

Early version, also known as pre-print

Link to publication record in Explore Bristol Research
PDF-document

University of Bristol - Explore Bristol Research
General rights

This document is made available in accordance with publisher policies. Please cite only the published version using the reference above. Full terms of use are available: http://www.bristol.ac.uk/red/research-policy/pure/user-guides/ebr-terms/

Nonlinear Analysis of Lateral Loading During Taxiway Turns

James Rankin[*], Bernd Krauskopf[†],
and Mark Lowenberg[‡]
Faculty of Engineering, University of Bristol, Bristol, UK, BS8 1TR

Etienne Coetzee[§]
Landing Gear Systems, Airbus, Bristol, UK, BS99 7AR

Abstract

We present a general approach to assess an aircraft's performance during taxiway manoeuvres across the range of its operation. The main motivation for this work is to evaluate the suitability of the existing Federal Aviation Regulation for lateral loads experienced during turning manoeuvres. To this end, operating regions are defined in terms of parameters specifying the approach velocity and steering input for a generic turn that is representative of pilot practice. The limits of the operating regions represent the extremes of the aircraft's operation during turning as determined by the maximal lateral loading conditions identified in published studies of instrumented in-service passenger aircraft. The performance of the turn can be assessed over the entire operational range in terms of the actual loads experienced at individual landing gears. Recent studies by the Federal Aviation Administration of instrumented aircraft have been limited to investigating the lateral loads experienced at the aircraft's CG position. Our results show that this information is insufficient to predict the actual loads experienced by individual landing gears, especially for the nose gear which is found to experience considerably higher lateral loads than predicted by the corresponding loads at CG. We find a robustness in the results with respect to changes in the aircraft's mass and the criterion used to define the limits of the operating regions.

Nomenclature

$\delta_N(t)$	=	steering angle at time t, deg
δ_{fin}	=	target steering angle, deg
δ_{rate}	=	maximum steer rate, deg/s
D_{CG}	=	maximum deviation of CG position from turn centre-line, m
D_{NLG}	=	maximum deviation of NLG from turn centre-line, m
L	=	longitudinal lag, m
N_{CG}	=	scaled lateral load factor at CG, g
N_{NLG}	=	scaled lateral load at NLG, no units
N_{OLG}	=	scaled lateral load at OLG, no units
N_{ILG}	=	scaled lateral load at ILG, no units
R	=	turn radius, m
t_{fin}	=	steer ramp required time, m

[*]Department of Engineering Mathematics.
[†]Department of Engineering Mathematics.
[‡]Department of Aerospace Engineering.
[§]Systems Engineering Specialist, Landing Gear Systems.

V_{init}	=	initial velocity, m/s
V_{loss}	=	velocity lost during turn, %
X	=	lateral displacement, m
Y	=	longitudinal displacement, m

1 Introduction

The landing gears of commercial aircraft are subject to substantial lateral loads during taxiing. For example, when exiting the runway at relatively high velocity, it is necessary for the tyres to generate sufficiently large lateral forces to complete the manoeuvre. There is a trade-off between increasing the structural strength of a landing gear to accommodate larger loads and the associated weight penalty. Therefore, it is important to identify the maximal lateral load values and the conditions under which they occur. This information can be used to assess the suitability of current regulations, to inform the design of future aircraft and to improve operational practice.

The regulation imposed by the Federal Aviation Administration (FAA) on the lateral loads experienced during turning for the certification of new civil aircraft is specified in Federal Aviation Regulation (FAR) 25.495. Termed the 0.5g lateral acceleration criterion, the regulation has two key parts with regards to the lateral loads experienced at the aircraft's centre of gravity (CG) position. Firstly, the limit loads during steady turning must not exceed 0.5g laterally. Secondly, each gear must structurally be able to withstand half of its maximum static vertical load applied laterally. In the regulation there is an inherent assumption that the limiting lateral load of 0.5g is evenly distributed between the aircraft's landing gears. The FAA have expressed concerns about the suitability of this regulation for the certification of modern passenger aircraft; in particular, the regulation is perceived to be too conservative for larger aircraft that have more than two main landing gears [1, 2]. With the aim of evaluating the existing regulation, the FAA have instrumented in-service aircraft and carried out a series of extensive studies to determine the actual lateral loads experienced during ground manoeuvres [3, 4, 1, 2]; these studies are discussed below.

Due to considerations of both cost and safety in performing specific ground tests, it is advantageous to use computer modelling to extend and complement the FAA studies. Indeed, computer simulation has been used previously to study the dynamics of aircraft on the ground; examples are a series of investigations by Klyde et al. that use a combination of mathematical modelling and ground tests [5, 6, 7]. Another study by Khapane et al. investigates asymmetric landing and ground manoeuvres with a model implemented in the multibody systems package SIMPACK, which includes nonlinear effects [8]. A multibody systems approach has been used extensively in the study of vehicle dynamics [9, 10]. Nonlinearities play a significant role in the dynamics of aircraft on the ground, especially when studying behaviour close to or beyond the limits of normal operation. A previous study by the authors [11] used an industry-tested, nonlinear model implemented in the multibody systems package SimMechanics to identify regions of safe operation in terms of the control inputs of the aircraft. In contrast to existing work, the model was analysed with tools from nonlinear dynamics, specifically, a bifurcation analysis was performed. The focus of the work was a steady state analysis in which stability boundaries are detected and followed under variation of parameters. In a more recent study by the authors [12] a fully parametrised mathematical model was developed and validated against the existing SimMechanics model. The advantage of this aircraft model, which is also used here and discussed in Section 1.1, is that it allows direct access to all system states and parameters. Our previous study also investigated changes in the stability limits with respect to variation of operational parameters, such as the aircraft's mass and centre of gravity position.

The specific aim of this work is to investigate lateral loading during ground manoeuvres in order to assess the suitability of the regulation described above. First of all, it is necessary to give further details of the existing investigations carried out by the FAA. Ref. [3] provides a statistical analysis of flight and loads data from a specific in-service aircraft recorded over the course of more than $30,000$ flight hours. Included in the report is relevant usage data; for example, cumulative occurrences of lateral load factor recorded during different phases of the aircraft's ground operations. The later study [4] summarises and compares such data

recorded from a range of different size aircraft. The more recent study [1] focuses specifically on lateral loads during ground manoeuvres and makes improvements in terms of the presentation of the data. In particular, the data is organised by aircraft model to allow comparison between the lateral loads experienced during different ground phases. Figure 1, reproduced from Ref. [1], shows cumulative occurrences of lateral load per flight scaled in terms of the operating weight for a typical medium-sized passenger aircraft. The data is broken up into different phases of the aircraft's ground operation. We focus on the loads experienced during turning; the relevant data in this study is that recorded during the taxi-in, taxi-out, landing roll and runway turn-off phases. The maximal lateral load factor, scaled by aircraft weight, recorded during the taxi-out phase is 0.2g, during the taxi-in phase it is 0.19g, during the landing roll phase it is 0.25g, and during the turn-off phase it is 0.24g. For convenience, these phases are grouped together as follows. The taxi-out and taxi-in phases are grouped together, and denoted the taxi phase, because they consist of similar manoeuvres; the overall maximal lateral load factor for the taxi phase is 0.2g. The landing roll and turn-off phases are grouped together and denoted the runway turn-off phase. We include the landing roll, which immediately precedes the runway turn-off, in order to capture loads recorded as the turn-off manoeuvre is initiated. The overall maximal lateral load factor for the runway turn-off phase is 0.25g. Larger loads occur during runway turn-off due to greater velocities immediately after landing. The data from this study suggests that the regulation limit for the lateral load factor is conservative. The effect of asymmetric loading between the landing gears is not taken into account in Ref. [1] and information with regards to the conditions under which specific lateral load values are attained is limited. The most recent study [2] presents limited ground test data recorded from an instrumented large commercial aircraft with more than two main landing gears. The significance of asymmetric loading between the main landing gears is investigated, but no information is provided about the nose landing gear. For specificity, in the remainder of the paper, we compare our results with usage data from Ref. [3] and the scaled loads data for a specific medium-sized passenger aircraft from Ref. [1].

A general approach to evaluate an aircraft's performance across an entire operating region for specific turning manoeuvres is presented. We focus on two types of turning manoeuvre: a runway turn-off manoeuvre that corresponds to the runway turn-off phase data, and a taxiway-to-taxiway transition that corresponds to the taxi phase data. We consider the maximal lateral load factors for the two ground phases, identified above in the FAA report data, to represent a practical upper bound that is not exceeded for the respective turning manoeuvres. Due to the large size of the data sets represented by the FAA studies, we reason that the limit lateral load factors are not surpassed in the day-to-day operation of the aircraft. With the aim of studying the actual landing gear loads at the limits of operation, we define a parametrised turn in terms of the turn approach velocity and the steering input during the turn. Taking into account the runway and taxiway geometry, we are able to relate the parametrised turn directly to the two manoeuvres under consideration. Parameter values at which the limit lateral load cases occur are identified; based on this information operating regions are defined. We find the actual gear loads at the limits of the operating regions and, therefore, at the limit of the aircraft's operation. The maximal gear loads are found for the two types of manoeuvre and two different mass cases (operating weights). We study the effect of asymmetric lateral loading between all the landing gears and the effect of different overall mass on the actual gear loads experienced. We find that the lateral load factor at CG is sufficient for the prediction of the maximal loads at the main landing gears, but not sufficient for the prediction of loads at the nose gear. Furthermore, we find that the loads at the nose gear are significantly underestimated by the lateral load factor at CG. Our results suggest that, for the specific aircraft under consideration, the existing regulation is too conservative for the main landing gears, but this is not necessarily the case for the nose gear. Other regulations, for example the towing regulation FAR 25.509, may account for larger lateral loads on the nose gear; however, the result is still important with respect to fatigue loading. An advantage of the general approach presented is that the limits of operation can be defined in terms of any user specified criteria. As an example, we carry out a similar study with operating regions defined in terms of a criterion that ensures efficiency of the manoeuvres. Overall, the approach presented here gives insights into the conditions under which the maximal loading cases identified in the FAA data occur, and extended information about actual gear loads at the limits of operation. As we demonstrate, the approach is not limited to the study of the extremes

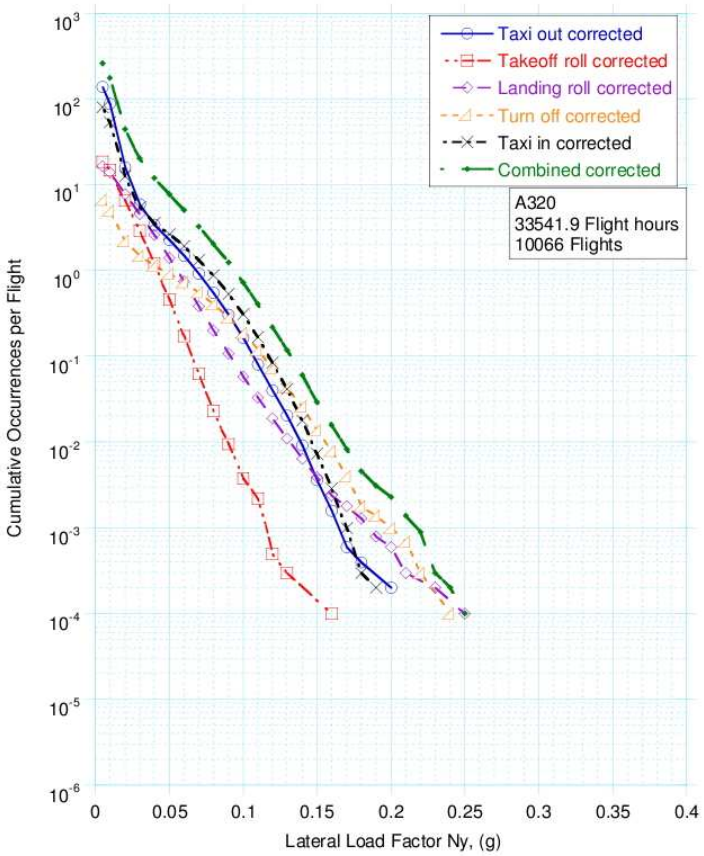

Figure 1: FAA instrumentation data (reproduction of figure A-27 from Ref. [1]) showing cumulative occurrences per flight of lateral load factor, corrected/scaled by operating weight corrected, separated into different ground phases.

of operation. Furthermore, although we focus on the loads experienced at individual landing gears, the approach is applicable for the study of any aircraft states of interest.

1.1 Mathematical model and specific loading cases

Our study utilises the fully parametrised mathematical model from Ref. [12] of a typical medium-sized, single-aisle passenger aircraft implemented in Matlab. The aircraft is modelled as a tricycle with the rigid airframe having three translational and three rotational degrees of freedom. The equations of motion were obtained via the balancing of forces and moments in each degree of freedom. Nonlinear effects are included in the tyre model [13], depending on tyre load and slip angle, and in the aerodynamic model, depending on velocity, angle of attack and sideslip angle of the airframe [14]. In addition to these nonlinearities in the models of local components, the equations of motion themselves are inherently nonlinear due to the dependence of the tyre forces and aerodynamic forces on the system states. A full description of the model and its validation against an established industry-tested SimMechanics model are provided in Ref. [12]. The advantage of using a low-order mathematical model is that it is computationally inexpensive to perform a larger number of simulations. Furthermore, the model allows direct access to component forces such as the lateral forces acting on individual landing gears. This allows for an analysis of the load distribution between

individual landing gears and a comparison of this information with loads experienced at the aircraft's CG position.

In this work we define two mass cases that allow for convenient comparison with the loads data presented in Ref. [1]. In the FAA study, the recorded lateral loads are scaled in terms of the aircraft's maximum landing weight (MLW) of 64560kg. In this paper the loads are scaled in the same way. A comparison of the load values reported in Ref. [1] before and after this scaling shows that the maximal lateral load cases correspond to a mass value of approximately 0.75×MLW= 48420kg, which is close to the minimal operating weight recorded in Ref. [3]. Therefore, we consider a heavy operating case at the MLW and a light operating case at 0.75×MLW. In the remainder of the paper we refer to the lateral load factor N_{CG} as the maximal lateral load N_y recorded at the aircraft CG position during the turn, scaled by the ratio of the operating weight (OR) with the MLW. So, the lateral load factor $N_{\mathrm{CG}} = \max(N_y) \times \frac{\mathrm{OR}}{\mathrm{MLW}}$. Throughout this paper we consider a forward CG position at 17% of the aircraft's Mean Aerodynamic Chord (MAC). In the results sections of this paper, the loads experienced at individual landing gears are discussed. For consistency, we scale the loads at the landing gears to allow direct comparison with loads at the CG position. The loads on the individual gears are normalised with respect to maximum vertical load on the gear under static loading. For the Nose Landing Gear (NLG) this corresponds to a heavy aircraft (at MLW) with a forward CG position; the corresponding vertical load under static loading is 92 kN. For the Main Landing Gears (MLGs) we consider a heavy aircraft with an aft CG position; the corresponding vertical load is 300 kN. In the results presented here, we assume that the aircraft always turns to the right and, therefore, in this case we can define the Outer Landing Gear (OLG) as the left-hand gear and the Inner Landing Gear (ILG) as the right-hand gear. We refer to the lateral gear load N_{NLG}, N_{ILG} or N_{OLG} as the maximal load recorded at the respective landing gear during the turn, divided by the static load values given above. For example, a lateral NLG load of $N_{\mathrm{NLG}} = 0.5$ corresponds to an actual load at the NLG of $0.5 \times 92\,\mathrm{kN} = 46\,\mathrm{kN}$.

The results in this paper are organised as follows. In Section 2 the parametrised turn is described. In Section 3 we find operational regions for different types of turn in terms of the parameters. In Section 4 the maximal lateral loads at the limits of the operational regions are determined. New operating regions are defined in Section 5 with respect to the efficiency of turns. Conclusions drawn from the results are presented in Section 6.

2 Generic parametrised turn

In this section a parametrised turn appropriate for the study of lateral loading during taxi manoeuvres is defined. The aim is to characterise a general turning procedure that is representative of pilot practice. Furthermore, for any given taxiway manoeuvre, there are a number of ways to perform that manoeuvre. Dependent on factors such as the velocity when entering a turn and steering characteristics, the lateral loads experienced during the manoeuvre vary significantly. The various factors discussed here are taken into account in the definition of a parametrised turn.

Typically, when the aircraft is approaching a turn on a straight section of taxiway the brakes are applied to achieve a desired velocity before entering the turn. After braking the turn is initiated with the application of steering. The velocity before entering the turn is represented here by the parameter V_{init} (with units m/s). In the simulations the initial condition describes the aircraft travelling in a straight line with the thrust set so that it is at equilibrium with fixed velocity V_{init}. From the initial condition the turn is initiated with the application of the steering; the steering angle is ramped up from 0° to a target value denoted δ_{fin} (given in degrees) which is taken as the second parameter to characterise the turn. The idealised steering profile used here is shown in Figure 2(a); it is represented by the function

$$\delta_N(t) = \frac{\delta_{\mathrm{fin}}}{2}\left[1 + \tanh\left(\frac{\delta_{\mathrm{rate}}}{\delta_{\mathrm{fin}}}\,(2t - t_{\mathrm{fin}})\right)\right],$$

where $\delta_N(t)$ is the steering angle applied at the nose gear at time t; furthermore, δ_{rate} is the fixed maximum steering rate and $t_{\mathrm{fin}} = \frac{3\delta_{\mathrm{fin}}}{\delta_{\mathrm{rate}}}$ is the required time to ramp up the steering such that $\delta_N(t_{\mathrm{fin}}) = \delta_{\mathrm{fin}}$. The

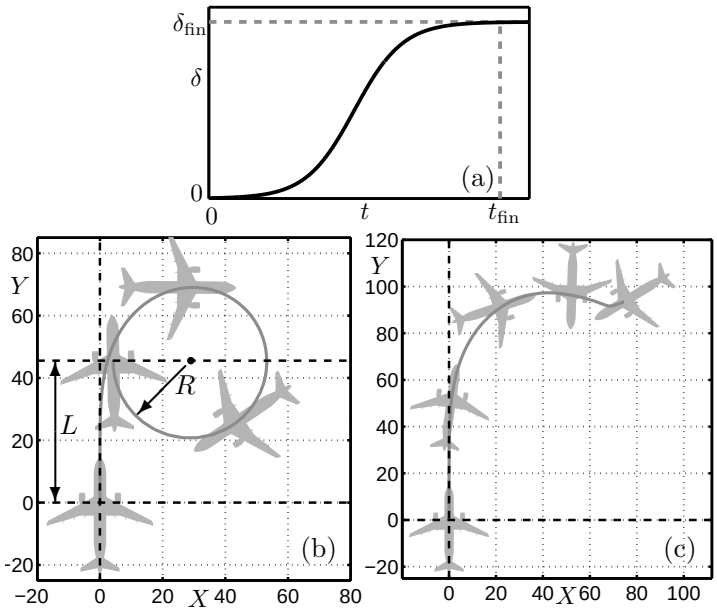

Figure 2: Panel (a) shows the steering profile, ramping up from 0° to the target steering angle δ_{fin} in time t_{fin}. Panels (b) and (c) show traces of the aircraft's CG (grey curve) for the parametrised turn with $(\delta_{\text{fin}}, V_{\text{init}}) = (29°, 11\text{m/s})$ and $(\delta_{\text{fin}}, V_{\text{init}}) = (29°, 15\text{m/s})$, respectively. In panel (a) $t = 0$ corresponds to the origin in panels (b) and (c). In panel (b) the black dot is the centre of the attracting turning circle with radius R. Dashed black lines illustrate the measurement of the lag L during convergence to the turning circle. In panel (c) the aircraft loses lateral stability and at the final point in the trajectory it is stationary.

realistic value of $\delta_{\text{rate}} = 12\text{deg/s}$ is used and the maximum rate is achieved at $t = \frac{t_{\text{fin}}}{2}$.

In the remainder of this section we study the properties of the parametrised turn for different values of the parameter pair $(\delta_{\text{fin}}, V_{\text{init}})$ of target steering angle and initial velocity. We initially study the resulting trajectories independently of the taxiway geometry, and in Section 3 we relate the trajectories directly to taxiway geometry. Each simulation gives a trajectory describing the motion of the aircraft over the (X, Y)-ground plane and associated time history data for the system states; the coordinates X and Y are given in metres (m). It is straight-forward to extract detailed information from the model, such as the forces experienced at the ground-tyre interactions.

A previous study by the authors identified two possible types of behaviour; when the aircraft makes a turn it can either converge to a stable turning circle solution or, if the manoeuvre is too aggressive, there is a loss of lateral stability [11]. Figure 2(b) and (c) are two example trajectories; plotted is a trace of the aircraft's CG position (grey curve) over the (X, Y) ground-plane with markers plotted to scale at equally spaced time intervals that indicate the aircraft's orientation along the trajectory. Figure 2(b) shows a trajectory computed for $(\delta_{\text{fin}}, V_{\text{init}}) = (29°, 11\text{m/s})$, for which the aircraft converges to a stable turning circle after a transient period. Illustrated are two quantities that describe the geometry of a stable trajectory. The radius of the turning circle to which the aircraft converges is denoted R (with units m). The longitudinal distance travelled from the initiation of the steering ramp at $t = 0$ to the point where the centre of the turning circle is passed is referred to as the approach lag; it is denoted L (with units m). For illustrative purposes, the parameter values of δ_{fin} and V_{init} for the trajectory shown in Figure 2(b) were chosen to exaggerate L. In general, when δ_{fin} is increased the radius R decreases as the aircraft follows tighter turns; when either δ_{fin} or V_{init} is increased the lag L increases as there is a longer delay before the aircraft makes the turn. Figure 2(c) shows a manoeuvre computed for $(\delta_{\text{fin}}, V_{\text{init}}) = (29°, 15\text{m/s})$; with this greater initial velocity the aircraft

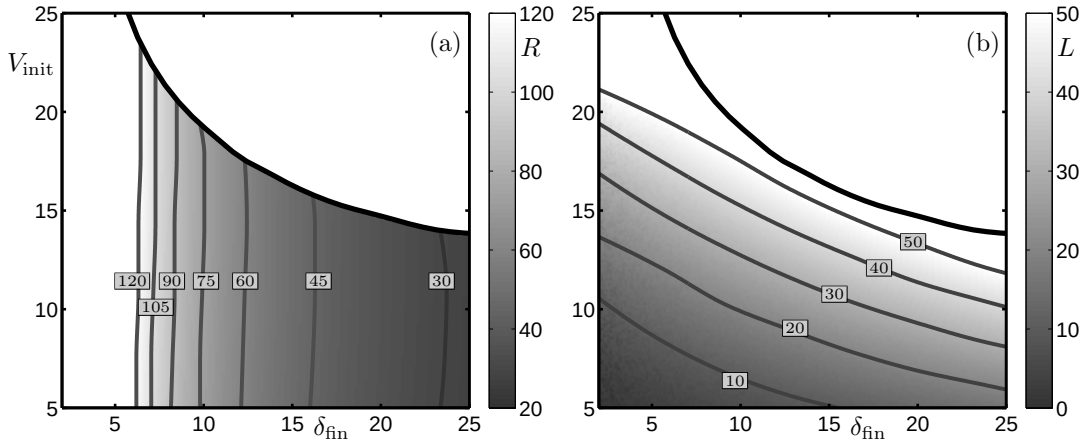

Figure 3: Greyscale maps showing values of turn radius R in panel (a) and approach lag L in panel (b) over the shown range of V_{init} and δ_{fin} values; contours are plotted in grey. The thick black curve is the limit of stable turning; white points above it correspond to laterally unstable turns.

loses lateral stability. This laterally unstable behaviour has been studied at length in reference [11]; here we identify the boundary between the two types of behaviour but the main focus is on stable turning.

2.1 Trajectory geometry

The implementation of a relatively low-order model in Matlab allows for the computation of large numbers of model simulations across a two-dimensional parameter space at low computational cost. A 200×200 grid of values for the parameters δ_{fin} and V_{init} is taken over the ranges $\delta_{\text{fin}} \in (2°, 25°)$ and $V_{\text{init}} \in (5, 25)$m/s. The velocity range is chosen to cover values representing relatively low-speed turns up to values in excess of the limits of operation. The maximal V_{init} values correspond to a thrust level of approximately 6% of maximum available thrust for the light mass case, and 7% for the heavy mass case. An aircraft trajectory as described in the previous section is computed for each of the 200×200 initial conditions in the $(\delta_{\text{fin}}, V_{\text{init}})$-plane. Various data is recorded and represented by greyscale maps over an appropriate range. Figure 3 shows the geometrical measures R and L over the grid of $(\delta_{\text{fin}}, V_{\text{init}})$-values in panels (a) and (b), respectively. For each value of δ_{fin}, simulations are performed at discrete values of V_{init} increasing from $V_{\text{init}} = 5$m/s to $V_{\text{init}} = 25$m/s and points at which there is a transition from stable solutions to laterally unstable solutions are detected. Specifically, if the lateral velocity of the aircraft exceeds 5m/s then this indicates that lateral stability has been lost. This choice of lateral velocity is consistent with our previous study [11] as a value for which the aircraft has been subject to a loss of lateral stability. The transition occurs along the black curve in each of the panels in Figure 3; white points that lie above this curve correspond to laterally unstable turns. Figure 3(a) shows that the turn radius R decreases with an increase in δ_{fin}. Note that it is independent of the initial condition determined by V_{init}, which follows from the fact that R is a measure of the stable turning circle solution to which the trajectories converge. Furthermore, the small changes in thrust used to set V_{init} do not affect R. However, V_{init} has a significant effect on the transient behaviour before convergence to a stable turning circle. This is reflected in Figure 3(b), which shows that the distance or lag L travelled by the aircraft before convergence to a stable turning circle increases with V_{init}. Recall that L increases with V_{init} because, with a greater initial velocity, the aircraft will travel further before executing the turn. There is also an increase in L with δ_{fin} because the steering rate is limited; it takes longer for the steering ramp to reach the target steering angle with increased δ_{fin}.

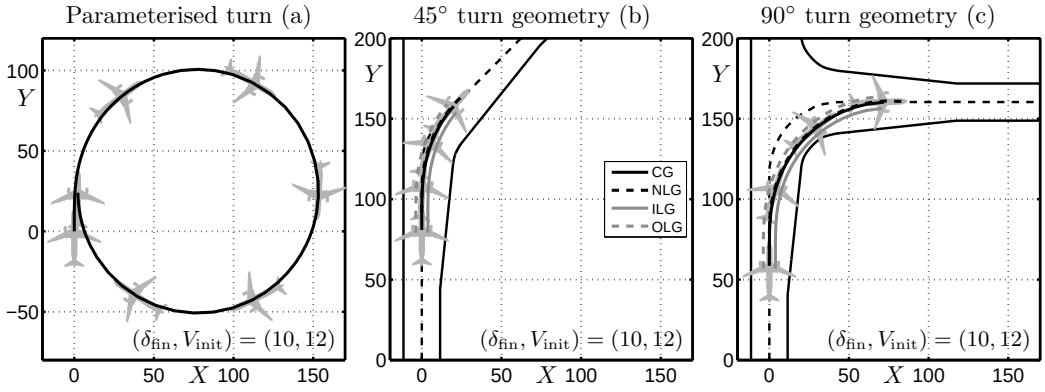

Figure 4: Panel (a) shows the aircraft trajectory for the parametrised turn at $(\delta_{\text{fin}}, V_{\text{init}}) = (10°, 12\text{m/s})$ plotted over the (X, Y)-ground plane; the aircraft has turned through 360° at the end of the trajectory. Panels (b) and (c) show the taxiway geometry for 45° and 90° turns with the taxiway limits plotted as solid black curves and the turn centre-lines plotted as dashed black curves. In each case the respective section of the parametrised turn is plotted; the trajectories end when the aircraft has turned through 45° and 90° in panels (b) and (c), respectively.

3 Operating region for typical taxiway turns

In this section we identify operating regions for different types of turning manoeuvre. The aim is to define the regions such that they represent a range of possible ways in which the different manoeuvres are performed. The first step is to relate the parametrised turn described in Section 2 to specific turning manoeuvres. Typical taxiway geometries are chosen that are representative for the turning manoeuvre under consideration. In Section 3.1 we identify bounds that restrict our study to parameter values for which the aircraft follows a trajectory suitable for the specific taxiway geometry. These bounds ensure that the operating region only consists of parameter values for which the aircraft remains safely within the taxiway geometry and does not excessively overshoot the turn. The second step is to ensure that the parameter values in the operating region do not exceed other criteria for practical turns. In Section 1 we concluded that the maximal lateral load factors at CG reported in the FAA studies in Ref. [1] are a practical upper bound for the operation of the aircraft. The criterion chosen in Section 3.2 is that the lateral load factor during the turn does not exceed the values in the FAA studies for the different types of manoeuvre.

3.1 Relating parametrised turn trajectories to specific manoeuvres

We describe a general method to relate the parametrised turn output trajectories directly to manoeuvres performed whilst exiting the runway and moving between taxiways. Each trajectory output is effectively fitted to the taxiway geometry upon which the manoeuvre is performed. The initial point in the trajectory is aligned to the entrance vector of the turn and the point on the trajectory at which the aircraft has rotated sufficiently to complete the turn is aligned with the exit vector of the turn. This works on the reasonable assumption that the steering is applied by the pilot at the appropriate distance from the turn entrance. Furthermore, it is assumed here that, if the end point of the aircraft's trajectory is approximately tangential to the exit vector of the turn, then it is possible to straighten out the aircraft to exit the turn. In this way, we are able to relate the data from a single computation at a specific value of δ_{fin} and V_{init} to any turn geometry.

We focus on two types of turning manoeuvre: the runway turn-off manoeuvre and a taxiway-to-taxiway

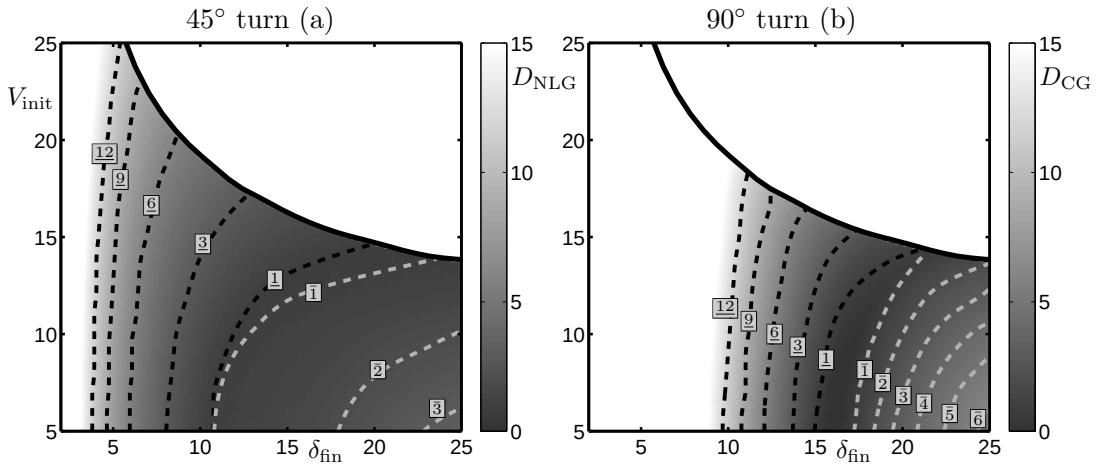

Figure 5: Greyscale maps showing D_{NLG} for the 45° turn (a) and D_{CG} for the 90° turn (b). Contours of D_{NLG} and D_{CG} plotted as dashed black curves represent an undershoot of the turn centre-line and are labelled with an underlined value; similarly, contours to the right plotted as dashed grey curves represent an overshoot of the turn centre-line and are labelled with a bar over the value.

transition. For simplicity we consider the single taxiway geometry of a 45° turn at a group V category airport [15] to be representative of a shallow runway turn-off manoeuvre. We choose the group V category as the standard airport geometry for which manoeuvrability studies are performed. Secondly, we consider a 90° turn at a group V category airport to be representative of the taxiway-to-taxiway transition. To allow for direct comparison the turn radius is 45m for both geometries. We now demonstrate the method described above by relating a single output trajectory to two different turning manoeuvres. Figure 4(a) shows the output trajectory of the parametrised turn for $(\delta_{\text{fin}}, V_{\text{init}}) = (10°, 12\text{m/s})$ plotted over the (X, Y)-ground plane; the aircraft has turned through 360° at the end of the trajectory. Panels (b) and (c) show the geometry for a 45° and a 90° turn, respectively. The taxiway limits are plotted as solid black curves and the turn centre-lines, straight sections of which correspond to the entrance and exit vectors of the turn, are plotted as dashed black curves. In each case a section of the parametrised turn is plotted over the taxiway geometry; the trajectories end when the aircraft has turned through 45° or 90°, as appropriate. Traces of the aircraft's CG position and the path of each landing gear are shown. For the same values of $(\delta_{\text{fin}}, V_{\text{init}}) = (10°, 12\text{m/s})$, the parametrised turn corresponds to following the turn centre-line closely for the 45° turn and the ILG almost exiting the taxiway for the 90° turn.

The pilot can ensure that the ILG remains a safe distance from the edge of the taxiway by following the turn centre-line with either the NLG or the approximate aircraft CG position. The former approach of following the turn centre-line (painted on the taxiway) with the NLG is used for shallow turns such as the 45° turn that we consider here. In particular, when turning at speed this method allows the pilot to control the turn easily as the NLG is approximately at the same position as the cockpit. Therefore, to study the 45° turn we define D_{NLG} (in m) as the maximum deviation of the NLG from the turn centre-line; for the trajectory shown in Figure 4(b) the NLG slightly undershoots the turn and $D_{\text{NLG}} \approx 2.5$m. For a 90° turn the pilot aims to follow the turn centre-line with the approximate position of the aircraft's CG; this ensures that the ILG does not come close to the edge of the taxiway even for a tight turn. Therefore, to study the 90° turn we define D_{CG} (in m) as the maximum deviation of the CG position from the turn centre-line; for the trajectory shown in Figure 4(c) the aircraft significantly undershoots the turn and $D_{\text{CG}} \approx 12.5$m. The aircraft should operate such that all landing gears are at least 4.5m from the edge of the taxiway as specified by the design of the taxiway geometry [15]; here we relax this to 3m to capture turns that marginally exceed the safety limit. In the trajectory shown in Figure 4(c) the ILG comes within 3m of the edge of the taxiway.

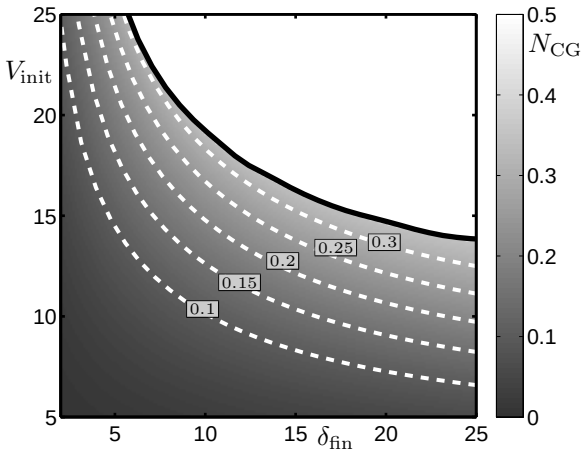

Figure 6: Greyscale map of the maximal lateral load factor N_{CG} for the output trajectory initialised from each $(\delta_{\text{fin}}, V_{\text{init}})$-pair; dashed white curves are contours of N_{CG}.

We use the two properties D_{NLG} and D_{CG} to determine bounds that identify suitable trajectories in the $(\delta_{\text{fin}}, V_{\text{init}})$-plane. Specifically, a left-hand bound on δ_{fin} and V_{init} ensures that the ILG does not come too close to the edge of the taxiway. A right-hand bound on δ_{fin} and V_{init} ensures that the aircraft does not overshoot the turn centre-line (with the NLG in the 45° turn or the CG in the 90° turn). An excessive overshoot of the centre-line is prohibited as this corresponds to the aircraft following a turn of unnecessarily small radius. Although the quantities D_{NLG} and D_{CG} are closely related, it is convenient to consider them separately for the two different turns.

Figure 5(a) and (b) show greyscale maps of D_{NLG} for the 45° turn and D_{CG} for the 90° turn, respectively. Contours of D_{NLG} and D_{CG} plotted as dashed black curves represent an undershoot of the turn centre-line and are labelled with an underlined value. Similarly, contours to the right plotted as dashed grey curves represent an overshoot of the turn centre-line and are labelled with a bar over the value. In Figure 5(a) there is a dark central region bounded by the curves $D_{\text{NLG}} = \underline{1}\text{m}$ and $D_{\text{NLG}} = \bar{1}\text{m}$ that represents the trajectories for which the NLG closely follows the turn centre-line (within ±1m). Similarly, in Figure 5(b) the region bounded by the curves $D_{\text{CG}} = \underline{1}\text{m}$ and $D_{\text{CG}} = \bar{1}\text{m}$ represents the trajectories for which the CG position closely follows the turn centre-line (within ±1m). The shading gets lighter to the left of the central region representing a greater undershoot and lighter to the right of the central region indicating a greater overshoot. Note that away from the central region the contours are closer together for the 90° turn because the aircraft must follow the turn centre-line for longer. We now define the operational limits for the two turn cases in terms of δ_{fin} and V_{init} by identifying specific contours in Figure 5. For the 45° turn the contour $D_{\text{NLG}} = \underline{12}\text{m}$ provides the left-hand bound, which ensures that the ILG remains at least 3m from the edge of the taxiway. The contour $D_{\text{NLG}} = \bar{1}\text{m}$ provides the right-hand bound, which ensures that the aircraft does not excessively overshoot the turn centre-line. Similarly, we define the bounds for the 90° turn as $D_{\text{CG}} = \underline{12}\text{m}$ and $D_{\text{CG}} = \bar{1}\text{m}$. Again, these bounds ensure that the ILG remains at least 3m from the edge of the taxiway and the aircraft does not excessively overshoot the turn centre-line. From a practical point of view the undershoot criteria are more important. The bounds identified here are used to define an operational region in terms of δ_{fin} and V_{init} in Section 3.2.

3.2 Maximal lateral loading conditions and operating region

We now identify values of the parameters δ_{fin} and V_{init} that coincide with trajectories for which the aircraft experiences the limiting lateral load factors reported in Ref. [1]. Recall from Section 1 that the maximal

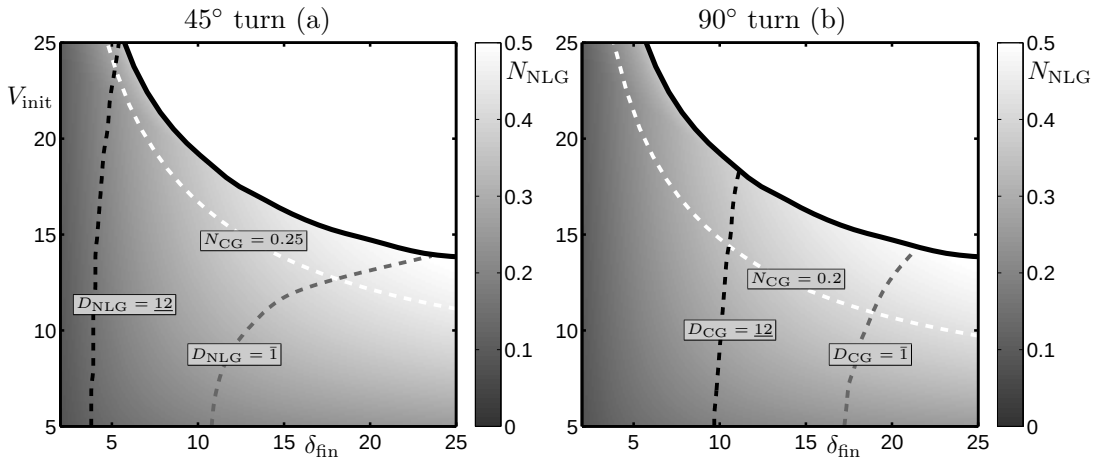

Figure 7: Greyscale maps show the lateral NLG load N_{NLG} for the trajectory represented by each $(\delta_{\text{fin}}, V_{\text{init}})$-pair. The operating regions are represented by the values of δ_{fin} and V_{init} that lie inside bounds on D_{NLG}, D_{CG} and N_{CG} as shown.

lateral load factor recorded for the aircraft under consideration is 0.25g during the runway turn off phase and 0.2g during the taxi phase. Therefore, the aim here is to determine values of the parameters δ_{fin} and V_{init} for which lateral load factor generated is 0.25g for a 45° turn and 0.2g for a 90° turn. This information describes an upper bound on the operation of the aircraft during taxiing for the two types of turn.

Figure 6 shows a greyscale map of the lateral load factor N_{CG} for the trajectory represented by each $(\delta_{\text{fin}}, V_{\text{init}})$-pair; dashed white curves show contours of N_{CG}. The figure shows that for turns performed at high velocity, the lateral load factor increases rapidly with increased steering angle. Conversely, at lower velocities N_{CG} increases slowly with increased steering angle. The lateral stability boundary appears to coincide with a limit lateral load factor of approximately 0.35g. Note that for all the aircraft considered in Refs. [4, 1, 2] the lateral load factor does not exceed 0.35g. With increasing N_{CG} the contours bound a larger region; this property that N_{CG} increases as the lateral stability boundary is approached is important. In general, for any aircraft, an increase in the lateral load factor with increased V_{init} or δ_{fin} is expected: when following a steady turning circle then $N_{\text{CG}} \propto \frac{V^2}{R}$ (or approximately, $N_{\text{CG}} \propto V^2 \times \delta$), where V is the aircraft's velocity and R is the radius of the turning circle corresponding to the steering angle δ.

From the maximal lateral load values in the FAA studies we can infer that for the runway turn-off manoeuvre the aircraft's operation corresponds to values of δ_{fin} and V_{init} below the 0.25g contour. Similarly, for taxiway-to-taxiway transitions the aircraft's operation corresponds to values of δ_{fin} and V_{init} below the 0.2g contour. We use this information in conjunction with the bounds defined in terms of D_{NLG} and D_{CG} to define operating regions for the two types of turn.

Figure 7(a) and (b) show the resulting operating regions for the 45° turn and the 90° turn, respectively. The left-hand limits of the operating regions shows that for increasing degree of turn, a larger δ_{fin} is required to keep the ILG a suitable distance from the edge of the taxiway; compare $D_{\text{NLG}} = \underline{12}$ in panel (a) with $D_{\text{CG}} = \underline{12}$ in panel (b). Again, the right-hand limit occurs at higher values of δ_{fin} with increased degree of turn. A larger steering angle is required for the NLG or CG position to follow the turn centre-line and, for the 90° turn, the aircraft must follow the centre-line for longer; compare $D_{\text{NLG}} = \bar{1}$ in panel (a) with $D_{\text{CG}} = \bar{1}$ in panel (b). For the 45° turn, the bound on N_{CG} is at larger values of δ_{fin} and V_{init} and closer to the lateral stability boundary; compare $N_{\text{CG}} = 0.25$ in panel (a) with $N_{\text{CG}} = 0.2$ in panel (b). Due to the larger velocities associated with the runway turn-off manoeuvre (45° turn), the corresponding lateral load factor is larger than during taxiway-to-taxiway transitions (90° turn). The operating regions are plotted over a greyscale map of the lateral NLG load N_{NLG}. It is convenient to show this information because the

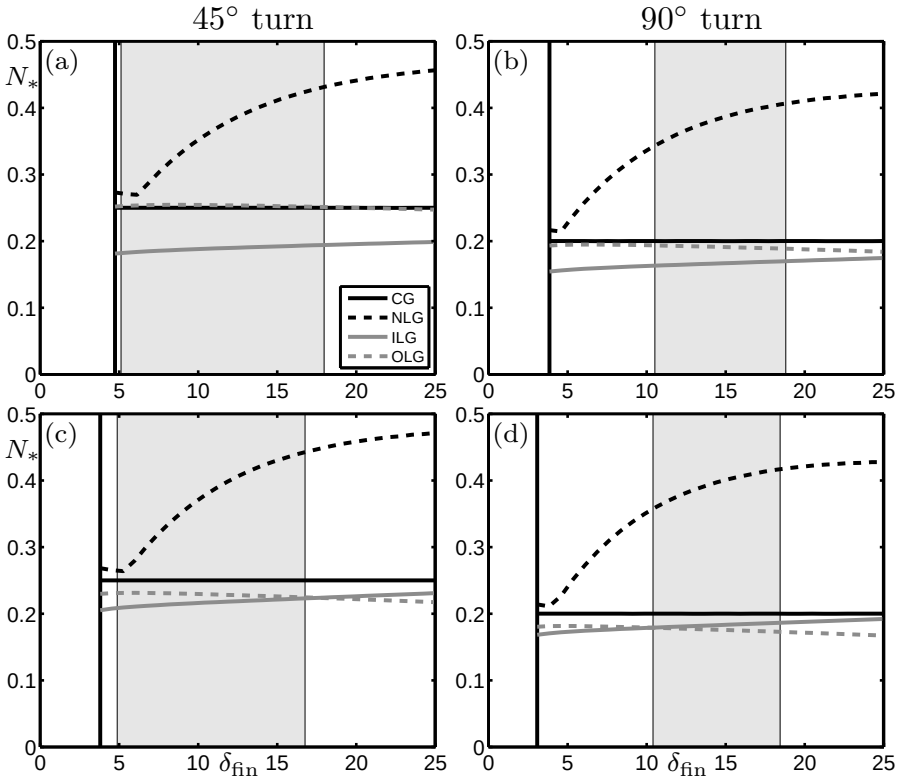

Figure 8: The lateral loads N_* (at CG, NLG, ILG and OLG) computed along the N_{CG} boundary curves and parametrised in terms of δ_{fin}. Panels (a) and (b) show data for the light aircraft case and panels (c) and (d) for the heavy aircraft case; turn degree is indicated at the top of the figure. In each panel the region shaded in grey represents the values of δ_{fin} corresponding to the appropriate operating region as shown in Figure 7. A vertical black line indicates the lower extent of the parametrised N_{CG} curve.

maximal landing gear loads across each operating region are studied in Section 4. We choose N_{NLG} because the lateral NLG loads come closest to exceeding the FAR. Note that the values of N_{NLG} are independent of the degree of the turn because the maximal loads on the NLG occur whilst the steering is being ramped up to δ_{fin}; this is before the aircraft has turned through 45° (the same holds for the ILG and OLG within the operating regions). The operating region for the 45° turn encompasses values of δ_{fin} and V_{init} corresponding to values of N_{NLG} that are close to the regulation's limit of $N_{\text{NLG}} = 0.5$. An important feature of the data shown in Figure 7 is that for both operating regions N_{NLG} is uniformly increasing as δ_{fin} and V_{init} approach the N_{CG} boundary. This property also holds for lateral ILG and OLG loads. Therefore, to find the maximal lateral gear loads in a given operating region it is sufficient to study the loads solely along the N_{CG} boundary.

4 Maximal lateral gear loads in operating regions

Since the maximal lateral gear loads in each operating region are attained at the N_{CG} boundary, we parametrise the N_{CG} curve to get a representation of the maximal lateral gear loads in the operating regions depending on δ_{fin}. Effectively the problem of finding the limiting loads has been reduced to computing these values along a one-dimensional curve. Given that the criteria for defining a region of standard operations can be applied to any aircraft configuration, the limiting loads are computed for light and heavy aircraft

cases. For both mass cases and the two types of taxiway turn, the lateral gear load values are found along the corresponding N_{CG} boundary at 50 discrete values of δ_{fin}. In this way, the lateral gears load values are extracted along the operating limit curves in Figure 7.

Figure 8 shows plots of the lateral gear loads N_* recorded along the N_{CG} limit parametrised in terms of δ_{fin}. The top two panels (a) and (b) represent the light aircraft case for which the operating regions are shown in Figure 7; the bottom panels represent the heavy aircraft case. The first column corresponds to the 45° turn and the second column to the 90° turn. In each panel the (fixed) value of N_{CG} is plotted as a reference. In each panel of Figure 8 vertical black lines indicate the δ_{fin} value corresponding to the lower extent of the N_{CG} curve; the section shaded grey represents the values of δ_{fin} corresponding to the appropriate operating region. The limits of the grey region correspond to intersections between N_{CG} and the appropriate D_{NLG} and D_{CG} curves.

First, we focus on the distribution of lateral loads between the ILG and the OLG. The lateral ILG and OLG loads are closely related to the lateral load factor N_{CG}: N_{ILG} and N_{OLG} vary linearly with δ_{fin} in all panels of Figure 8. Panels (a) and (b) show that, in the light case, for both types of turn, N_{OLG} is larger than N_{ILG}. Within the operating region for the 45° turn N_{OLG} is at most 40% larger than N_{ILG}; for the 90° turn the difference is at most 20% larger. This difference can be accounted for by the fact that during a turn the aircraft's weight shifts to the outside gear and the OLG takes a larger vertical load; in general the lateral load generated by a tyre increases with vertical load. In the heavy aircraft case, for both types of turn, there is a value of δ_{fin} above which N_{ILG} is larger than N_{OLG}; see panels (c) and (d). Due to the aircraft geometry the ILG generates a larger slip angle whilst turning. For stable turns the lateral forces generated by the tyres increase with slip angle and in the heavy case there is some value of δ_{fin} for which this effect dominates over the larger vertical load at the OLG. For a heavy aircraft in the operating region for the 45° turn $N_{\mathrm{OLG}} > N_{\mathrm{ILG}}$ with the values becoming equal at the maximal value of δ_{fin}; see panel (c). Conversely, in the operating region for the 90° turn, $N_{\mathrm{ILG}} > N_{\mathrm{OLG}}$ with the values being equal at the minimal value of δ_{fin}; see panel (d). Across all four cases shown in Figure 8, the lateral load factor is a good predictor of the lateral ILG and OLG loads. Furthermore, N_{ILG} and N_{OLG} are less than or equal to the lateral load factor at CG (with a slight exception for the OLG in Figure 8(a)).

Across all four cases shown in Figure 8 the lateral NLG loads N_{NLG} are greater than N_{OLG}, N_{ILG} and N_{CG}. The loads at the NLG increase with δ_{fin} and the maximal values occur at the upper limit of δ_{fin}. In the operating regions for the 45° turn N_{NLG} is approximately equal to N_{CG} for small values of δ_{fin}; see panels (a) and (c). However, as δ_{fin} increases there is a rapid deviation and the lateral NLG load is vastly underestimated by the lateral load factor at CG. Furthermore, at the upper limit of δ_{fin} the loads at the NLG come close to $N_{\mathrm{NLG}} = 0.5$, which is approaching the limit imposed by the FAA. For all values of δ_{fin} in the operating regions for the 90° turn N_{NLG} is vastly underestimated by N_{CG}; see panels (b) and (d). At the upper limit of δ_{fin} the loads at the NLG are underestimated by a factor of two. We conclude that studying the lateral load factor at CG alone is insufficient for the prediction of the loads at the landing gears. Note that the large change in mass between the light and heavy cases corresponds to only a marginally increased lateral NLG load. The largest loads at the OLG occur for the light mass case.

5 Operating region for efficient turns

In Sections 3 and 4 the upper limit of operation was defined in terms of the maximal lateral load factors shown in Figure 1. In this way, the limits of the operating regions represent the extremes of the aircraft's operation. However, the approach presented in this paper is very flexible and other limits can be defined in a similar way with any relevant criteria that provide a bound within which it is desirable for the aircraft to operate. As an example, we now define operating regions in terms of a target for the efficiency of turns. Specifically, a turn can be considered efficient if during the turn a large proportion of the approach velocity is conserved.

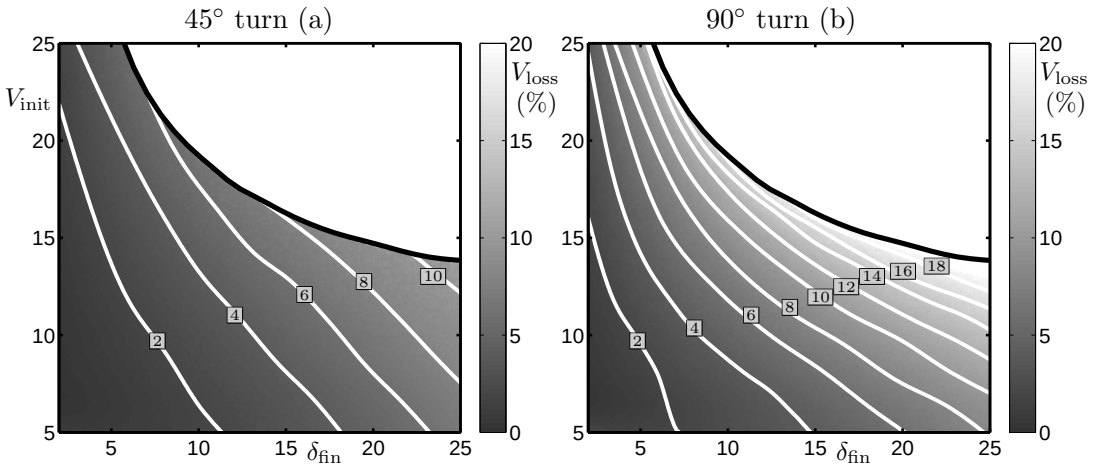

Figure 9: Greyscale maps showing the percentage of velocity lost V_{loss} for the two types of turn for the trajectory represented by each $(\delta_{\text{fin}}, V_{\text{init}})$-pair. White curves are contours of V_{loss}.

The velocity lost during a turn, V_{loss}, is expressed as a percentage by the equation

$$V_{\text{loss}} = 100 \times \frac{V_{\text{init}} - V_{\text{fin}}}{V_{\text{init}}},$$

where V_{fin} is the velocity of the aircraft when it reaches the exit vector of the turn. For smaller values of V_{loss} less velocity is lost and the turn is more efficient. Figure 9 shows greyscale maps of V_{loss} for the two types of turn; contours of V_{loss} are plotted as white curves. The plots show that more velocity is lost with a higher-degree turn. Specifically, in panel (a) we see that for the 45° turn the maximal value of V_{loss} just exceeds 10% in the stable region; the largest value occurs close to the lateral stability boundary at high δ_{fin}. For the 90° turn, see panel (b), the maximal value of V_{loss} just exceeds 18% with the maximal values occuring close to the lateral stability boundary. The relative spacing between the contours for the two types of turn shows that there is a larger penalty in terms of efficiency when increasing δ_{fin} and V_{init} for the 90° turn. Therefore, depending on the type of turn, different V_{loss} limits are chosen as the criteria for suitably efficient manoeuvres.

We now specify contours of V_{loss} to represent upper limits for new operating regions that, as in Section 3.2, take into account appropriate limits for D_{NLG} and D_{CG}. An upper limit of $V_{\text{loss}} = 4\%$ is taken for the 45° turn and $V_{\text{loss}} = 8\%$ for the 90° turn. These limits are chosen such that in these new operating regions the lateral load factor does not exceed the maximal values identified in the FAA studies for the light aircraft case. Accordingly, $N_{\text{CG}} < 0.25\text{g}$ along $V_{\text{loss}} = 4\%$ for the 45° turn, and $N_{\text{CG}} < 0.2\text{g}$ along $V_{\text{loss}} = 8\%$ for the 90° turn. The same V_{loss} limits are chosen for the heavy aircraft case to allow for direct comparison between the mass cases. Figure 10 shows the resulting operating regions, again plotted over a greyscale map of N_{NLG}. The new operating regions represent a subset of those defined in Section 3.2 due to the way in which the V_{loss} bounds are chosen.

The lateral load factor and lateral gear loads increase as the V_{loss} limit is approached and, therefore, in order to identify the maximal loads in the region we extract the loads along the V_{loss} curves. Plots of the lateral load factor and lateral gear loads are shown for the two types of turn and two mass cases in Figure 11. For the 45° turn, the lateral load factor N_{CG} peaks close to the lower extent of the operating region and steadily drops off as δ_{fin} increases; see panels (a) and (c). For the light case $N_{\text{OLG}} > N_{\text{ILG}}$ with the loads becoming equal at the upper extent of the operating region; see panel (a). For the heavy case there is a transition from the greater load being the OLG to the ILG with $N_{\text{ILG}} = N_{\text{OLG}}$ at $\delta_{\text{fin}} \approx 10°$; see panel (c). For the 90° turn, the lateral load factor decreases with increased δ_{fin} in the operating region; see panels

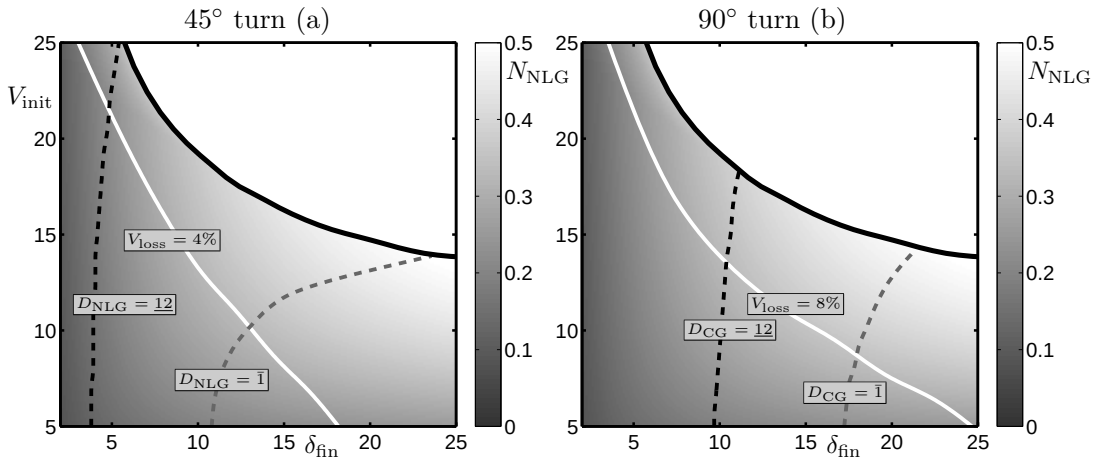

Figure 10: Greyscale maps showing the lateral NLG load N_{NLG} for the trajectory represented by each $(\delta_{\text{fin}}, V_{\text{init}})$-pair. The operating regions are the values of δ_{fin} and V_{init} that lie inside bounds on D_{NLG}, D_{CG} and V_{loss} as shown.

(b) and (d). For the light aircraft case $N_{\text{OLG}} > N_{\text{ILG}}$ with the loads becoming equal at the upper extent of the operating region; see panel (b). For the heavy case $N_{\text{ILG}} > N_{\text{OLG}}$ and the loads are equal at the lower extent of the operating region; see panel (d). For both turn types with the light case, N_{CG} matches N_{OLG} very closely and is a good predictor of the loads at the main landing gears; see panels (a) and (b). For the heavy case the main lateral gear loads are more evenly distributed; see panels (c) and (d). Again, in all cases N_{CG} is a good predictor for the loads at the main landing gears. However, the loads at the NLG are vastly underestimated by N_{CG}. The main qualitative difference between the profile of N_{NLG} when compared with Figure 8 is that with increasing δ_{fin} there is a peak value after which the load drops off; for the 45° turn this occurs at $\delta_{\text{fin}} \approx 12°$ and for the 90° turn at $\delta_{\text{fin}} \approx 16°$, independently of the mass case. The data shows that the inadequacy of N_{CG} in predicting N_{NLG} is not limited to the extremes of the aircraft's operation.

6 Conclusions

We presented a general approach to evaluate an aircraft's performance across an entire operating region for specific turning manoeuvres. The dynamic model of a tricycle-gear passenger aircraft used in this paper was fully validated against an industry-tested model in a previous study. A turn that represents pilot practice during taxiway manoeuvres was parametrised in terms of approach velocity and steering input. The output trajectories of the parametrised turn were then related directly to turning manoeuvres. Representative runway and taxiway geometries were chosen for two types of turning manoeuvre: a runway turn-off of 45° and a taxiway-to-taxiway transition of 90°. Operating regions were defined to represent a range of possible ways in which the different manoeuvres are performed where the limits of the regions represent the extremes of the aircraft's operation. Specifically, we considered the extremes of operation as given by the maximal lateral load factors (at the aircraft's CG position) reported in studies of in-service aircraft carried out by the FAA. Such operating regions were defined for the two types of manoeuvre and for two mass cases. In this way we assessed the performance, in terms of the actual lateral loads experienced, of individual landing gear across the operating regions. In particular, we focused on the maximal lateral loads at the limits of the operating regions.

The results show that the lateral load factor at CG is a good quantitative predictor of the loads experienced at the main landing gears. We investigated asymmetric lateral loading between the main gears and found that whether greater loads occur at the inner or outer gear depends on the turn type and the

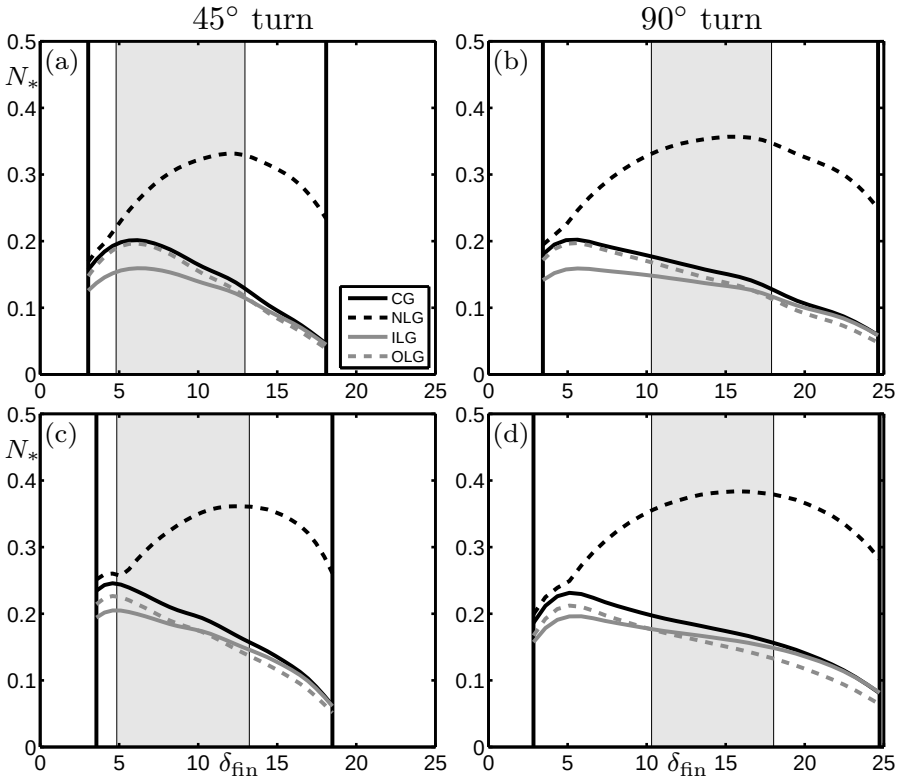

Figure 11: The lateral loads N_* (at CG, NLG, ILG and OLG) computed along the V_{loss} boundary curves parametrised in terms of δ_{fin}. Panels (a) and (b) show data for the light aircraft case and panels (c) and (d) for the heavy aircraft case; turn degree is indicated at the top of the figure. In each panel the grey shaded region represents the values of δ_{fin} corresponding to the appropriate operating region as shown in Figure 10; vertical black lines indicate the upper and lower extent of δ_{fin} for the parametrised V_{loss} curve.

aircraft mass. More significantly, the lateral loads at the nose landing gear are found to be vastly underestimated by the lateral load factor at CG, in the worst case by a factor of two. Another finding is that, for the same lateral load factor at CG, the actual lateral gear loads are largely unaffected by changes to the aircraft weight. We consider that an investigation into lateral loading during taxiing operations should not be confined to studying the lateral load factor at CG. Furthermore, should future studies be carried out with instrumentation of the individual landing gears, it is of paramount importance that the nose gear be included. In conjunction with existing studies, our results suggest that, for the particular aircraft under consideration, the limit imposed in the FAR is too conservative for the main landing gears.

To illustrate the generality of the approach described above, it was adapted to study lateral gear loads in operating regions based on a criterion for the proportion of the aircraft's approach velocity that is conserved during a turn. The main observation is still that the lateral load factor at CG is a good predictor of loads at the main gears, but a bad predictor of the loads at the nose gear. The robustness in the qualitative behaviour shows that the overall result is not limited to the extremes of the aircraft's operation. The criterion under consideration could easily be adapted to satisfy a specific safety margin for the landing gear loads with respect to regulation limits. Such a criterion could then be implemented through pilot practice or in an automatic control system. Our approach is suitable for the study of any reasonable criteria on the aircraft's operation; for example, speed limits depending on taxiway conditions, limiting vertical or lateral load on a specific gear, the maximal slip angles generated at the tyres, or a bound on the energy lost during manoeuvres. It can

also be applied to study performance with respect to changes in design. A particular example would be to efficiently assess the performance of different landing gear configurations for heavy aircraft with more than two main gears.

Acknowledgements

This research is supported by an Engineering and Physical Sciences Research Council (EPSRC) Case Award grant in collaboration with Airbus in the UK.

References

[1] Jones, T., Rustenburg, J., Skinn, D., and Tipps, D., "Study of Side Load Factor During Aircraft Ground Operations," Tech. Rep. DOT/FAA/AR-05/7, Federal Aviation Administration, U.S. Department of Transportation, Federal Aviation Administration, Office of Aviation Research, Washington, DC 20591, March 2005.

[2] Finn, E., Gleich, R., Green, K., Saccarelli, R., and Szot, M., "Investigation of Limit Design Lateral Ground Maneuver Load Conditions," Tech. Rep. DOT/FAA/AR-07/38, Federal Aviation Administration, U.S. Department of Transportation, Federal Aviation Administration, Office of Aviation Research, Washington, DC 20591, June 2007.

[3] Rustenburg, J., Skinn, D., and Tipps, D., "Statistical Loads Data for the Airbus A320 Aircraft in Commercial Operations," Tech. Rep. DOT/FAA/AR-02/35, Federal Aviation Administration, U.S. Department of Transportation, Federal Aviation Administration, Office of Aviation Research, Washington, DC 20591, April 2002.

[4] Tipps, D., Rustenburg, J., Skinn, D., and DeFiore, T., "Side Load Factor Statistics From Commercial Aircraft Ground Operations," Tech. Rep. UDR-TR 2002-00119, Federal Aviation Administration, U.S. Department of Transportation, Federal Aviation Administration, Office of Aviation Research, Washington, DC 20591, January 2003.

[5] Klyde, D., Myers, T., Magdaleno, R., and Reinsberg, J., "Identification of the dominant ground handling charactersitics of a navy jet trainer," *Journal of Guidance, Control, and Dynamics*, Vol. 25, No. 3, May 2002, pp. 546–552.

[6] Klyde, D., Sanders, E., Reinsberg, J., and Kokolios, A., "Flight test evaluation of a stability augmentation steering system for aircraft ground handling," *Journal of Guidance, Control, and Dynamics*, Vol. 27, No. AIAA-2003-5318, 2004.

[7] Klyde, D., Magdaleno, R., and Reinsberg, J., "The effect of tire pressure on aircraft ground handling," *Journal of Guidance, Control, and Dynamics*, Vol. 26, No. AIAA-2002-4798, July 2003, pp. 558–564.

[8] Khapane, D. P., "Simulation of asymmetric landing and typical ground maneuvers for large transport aircraft," *Aerospace Science and Technology*, Vol. 7, No. 8, December 2003, pp. 611–619.

[9] Blundell, M. and Harty, D., *The Multibody Systems Approach to Vehicle Dynamics*, SAE, September 2004.

[10] Shabana, A., *Dynamics of Multibody Systems*, Cambridge University Press, 2nd ed., October 2003.

[11] Rankin, J., Coetzee, E., Krauskopf, B., and Lowenberg, M., "Bifurcation and Stability Analysis of Aircraft Turning on the Ground," *AIAA Journal of Guidance, Control, and Dynamics*, Vol. 32, No. 2, March 2009, pp. 500–511.

[12] Rankin, J., Krauskopf, B., Lowenberg, M., and Coetzee, E., "Operational Parameter Study of Aircraft Dynamics on the Ground," *To appear in ASME Journal of Computational and Nonlinear Dynamics*, Vol. CND-09-1022, 2010.

[13] Pacejka, H. B., *Tyre and Vehicle Dynamics*, Elsevier, 2006.

[14] Jeanneau, M., "Description of aircraft ground dynamics," Garteur FM AG17 RP0412731, GARTEUR, 2004.

[15] FAA, "Airport Design," *Advisory Circular*, Vol. 150, September 1989, pp. 5300–13.